Pinch-off of liquid jets at the finite scale of an interface

Francisco Cruz-Mazo and Howard A. Stone

Phys. Rev. Fluids **7**, L012201 — Published 18 January 2022

DOI: 10.1103/PhysRevFluids.7.L012201

Pinch-off of liquid jets at the finite scale of an interface

Francisco Cruz-Mazo[1, 2, *] and Howard A. Stone[1, †]

[1] *Dept. Mechanical and Aerospace Engineering, Princeton University, Princeton, NJ 08544, USA.*
[2] *Dept. Ingeniería Aeroespacial y Mecánica de Fluidos, Universidad de Sevilla, 41092 Sevilla, Spain*

(Dated: January 5, 2022)

We derive self-similar continuum equations that govern the rupture of liquid threads at scales within the influence of interfacial dynamical effects. This regime and the obtained power-law solution for the evolution of the minimum neck radius, $h_{min} = 0.00107(t_b - t)^{2.34}$, fill a void in the literature in between the classical inertial-viscous regime and the stochastic formulation, and reconciles flow features such as asymptotic slow boundary conditions far away from the singularity and symmetric profiles, respectively. Due to its inherent ties to the production of monosized droplets from jetting, this work can be utilized to approach, for example, the study of electrosprays or flow focusing at these critical scales for aerospace nano-thruster technology or single biomolecule imaging with x-ray free-electron lasers.

The ubiquity of liquid jets in nature, and their generation, stability and controlled rupture have motivated not only fundamental research [1] but also their use in multidisciplinary endeavors in analytical chemistry [2], structural biology [3], and aerospace nano-propulsion [4] among others. Eggers [5] established the self-similar equations for the pinching process where inertia, surface tension and viscous terms are balanced: the inertial-viscous regime (IV). The evolution of the minimum neck radius h_{min} was found to be $h_{min}^{(IV)} = 0.03(\sigma/\mu)(t_b - t)$, where σ, μ and t_b are the surface tension, viscosity and time of break up, respectively. However, its range of validity is not universal as the pinch-off can be triggered upstream under a pure dominance of inertia or viscosity, although after an intermediate regime [6–8], the thread dynamics behaves according to the IV-regime [5].

However, Moseler and Landman [9] demonstrated via molecular simulations how the breakup of a liquid propane jet forced through a hole with a diameter of six nanometers does not obey the exponent and predictions based on the IV analysis. To address this limitation, a stochastic force was added to the slender jet model in order to identify a regime where thermal fluctuations from the bulk can control the pinching process (bT-regime). This approach was later exploited by Eggers [10] who derived numerically $h_{min}^{(bT)} \propto (t_b - t)^{0.418}$. Subsequently, researchers have studied the inclusion of vapor-pressure effects in molecular dynamic simulations [11], ultra-low surface tension experiments at much larger scales [12–14], and further numerical explorations regarding the validity of the 0.418-power-law for ultra-low surface tension [15].

Whether the power-law exponent is determined by the balance of inertia, viscous and surface tension stresses, or stochastic forces, these works share a common assumption no matter the length scale that is under study: an interface thickness δ such that $\delta/h_{min} \ll 1$. This simplicity has a profound implication for the interface dynamics,

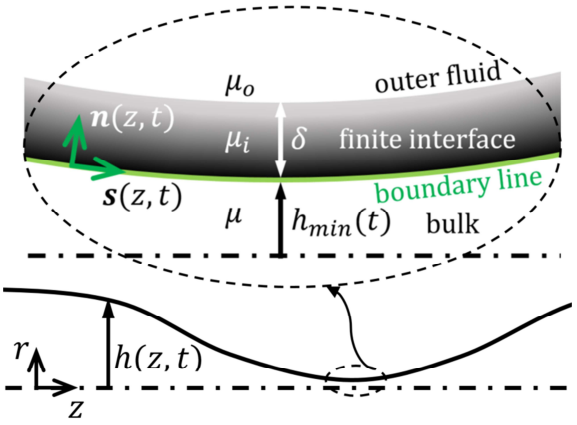

FIG. 1. Sketch about the minimum thickness of the pinching of a liquid thread. A detailed view in the vicinity of the minimum radius h_{min} and at a scale comparable in size to the interface thickness δ (in grey color gradient).

which is a frozen sharp layer that affects the jet behavior through the Laplace-Young stress with a certain value for σ.

However, the interface cannot be considered infinitely narrow under the following scenarios: (i) during the pinch-off of jets where eventually $\delta/h_{min} \sim 1$ or (ii) for thin enough steady liquid jets with a radius h_∞ such as $h_\infty \longrightarrow \delta$. It is then natural to ask: (i) does a finite interface produce intermediate spatio-temporal scales in between the IV- and bT- regimes? and, if so, (ii) would these novel scales lead to self-similar properties within the breakup of a liquid jet and, consequently, to a new power-law exponent for the dynamics of the minimum neck radius? In this work, we shed light on this matter by deriving an extended but analytically approachable slender model for a liquid jet that is affected by the finite thickness of the interface.

Model Formulation - We distinguish two domains, a liquid bulk and a finite phase-graded interface, which are separated by a non-material contact line as the axisymmetric surface function $r = h(z,t)$ (Fig. 1). The classical

* fcruz5@us.es
† hastone@princeton.edu

idea [1] that we utilize is that for a sufficiently slender jet (i.e. characteristic radial ℓ and axial L length scales are such as their ratio $\epsilon = \ell/L \ll 1$) higher-order terms are negligible and can be removed from the set of non-dimensional incompressible axisymmetric Navier-Stokes equations for the liquid bulk,

$$u_t + uu_r + vu_z = -\frac{p_r}{\epsilon^2} + \frac{u_{rr}}{\epsilon^2} + u_{zz} + \frac{u_r}{r\epsilon^2} - \frac{u}{r^2\epsilon^2} \quad (1a)$$

$$v_t + uv_r + vv_z = -p_z + \frac{v_{rr}}{\epsilon^2} + v_{zz} + \frac{v_r}{r\epsilon^2}, \quad (1b)$$

where subscripts denote partial derivatives. The axial z and radial r lengths, and time t have been, respectively, made dimensionless by the axial $L = \mu^2/(\rho\sigma)$ and radial $\ell = \epsilon L$ scales and the characteristic time $\tau = \epsilon^2\mu^3/(\rho\sigma^2)$. Note that p, u, v are measured in terms of ℓ, L, τ and the density ρ, with the units $\rho L^2/\tau^2$, ℓ/τ and L/τ, respectively. Additionally, μ/ρ is implicitly related to L and τ as $\tau \sim L^2\rho/\mu$. Given the radial $\mathbf{e}_r$ and longitudinal $\mathbf{e}_z$ cylindrical unit vectors, we radially expand in the bulk ($r < h(z,t)$) the dimensionless pressure $p(r,z,t)$ and velocity fields $\mathbf{v}(r,z,t) = u(r,z,t)\mathbf{e}_r + v(r,z,t)\mathbf{e}_z$ by using the aforementioned parameter $\epsilon = \ell/L \ll 1$; below we link with the finite interface as a matching condition in terms of its thickness δ and mobility M from the Cahn-Hilliard description.

We next take advantage of these previous standard ideas by the classical variable expansion

$$p(r,z,t) = p_0(z,t) + p_2(z,t)(\epsilon r)^2 + ... \quad (2a)$$

$$v(r,z,t) = v_0(z,t) + v_2(z,t)(\epsilon r)^2 + ... \quad (2b)$$

$$u(r,z,t) = -v_{0z}(z,t)\epsilon r/2 - v_{2z}(z,t)(\epsilon r)^3/4 + ..., \quad (2c)$$

that simultaneously satisfy mass conservation and the symmetry of the problem.

Once the Navier-Stokes equations are simplified with the variable expansion and after retaining the leading terms [1], the classical axial momentum equation is

$$v_{0t} + v_0 v_{0z} + p_{0z} = 4v_2 + v_{0zz}. \quad (3)$$

Both the bulk and finite-thickness interface flow together through a quiescent outer fluid with a density ρ_o and a viscosity μ_o that does not exert any external stress over the entire jet (Fig. 1). Thus, there is an inner balance of stresses between both domains through the boundary line that enables us to add the resulting net normal $f^{(n)}$ and shear $f^{(s)}$ stresses from the interface to the bulk at $r = h(z,t)$, leading to two dimensionless equations along the normal n and tangential s coordinates (see Fig. 1),

$$p - \frac{2\left[u_r + \epsilon^2 v_z h_z^2 - \left(v_r + \epsilon^2 u_z\right) h_z\right]}{1 + \epsilon^2 h_z^2} = f^{(n)} \quad (4a)$$

$$\frac{2\epsilon^2 h_z\left(u_r - v_z\right) + \left(v_r + \epsilon^2 u_z\right)\left(1 - \epsilon^2 h_z^2\right)}{\epsilon\left(1 + \epsilon^2 h_z^2\right)} = \epsilon f^{(s)} \quad (4b)$$

For the evaluation of $f^{(n)}$ and $f^{(s)}$ we utilize the Cahn-Hilliard formulation [16–18] for the fluid fraction ϕ, which is based on the behavior of the chemical potential $\theta = \phi^3 - \phi - \delta^2\nabla^2\phi$ that is formed by the competition between the phase separation, $\phi^3 - \phi$, and interface penalizing, $-\delta^2\nabla^2\phi$, terms

$$\phi_t + \left(\mathbf{v}^{(i)} - \mathbf{v}^{(s)}\right) \cdot \nabla\phi = \frac{3M\sigma}{2\sqrt{2}\delta}\nabla^2\left(\phi^3 - \phi - \delta^2\nabla^2\phi\right). \quad (5)$$

The difference of velocity components along n and s, respectively, from the inner interface $\mathbf{v}^{(i)} = u^{(i)}\mathbf{n} + v^{(i)}\mathbf{s}$ to the boundary streamline $\mathbf{v}^{(s)} = u^{(s)}\mathbf{n} + v^{(s)}\mathbf{s}$ are assumed to be of $O(\epsilon)$ due to the departures of the interface from a sort of frozen state. Next, we take advantage of the slenderness of the interface as $\delta \sim \ell \ll L$ and $\partial/\partial s \sim 1/L \ll \partial/\partial n \sim 1/\delta \sim 1/\ell$. Thus, we neglect shear derivatives for terms that involve $\nabla\phi$ (i.e, $\nabla \approx \mathbf{n}\partial/\partial n$). In addition, our expansion parameter can be scaled as $\epsilon \sim (3M\rho/2\sqrt{2}\tau)^{1/2}$ in order to enable compatibility of capillary waves along with the interface [18] as ϕ_t cannot be neglected. This scaling for ϵ should be seen as an equivalent squared Cahn number also estimated in [18]. Subsequently, this matching condition comes from the spatio-temporal coupling between both interface and bulk within the earliest stages of this pinch-off regime after leaving the equilibrium. Thus, we can utilize the viscous-capillary dimensional group to express interfacial parameters, as $\sigma/\ell \sim \rho L^2/\tau^2$. Then, $\phi(n,s,t)$ varies from the boundary line $r = h(z,t)$ (where $\phi = -1$) to the outer fluid ($\phi = 1$). With these simplifications, Eq. (5) then relates the second-order derivative of the chemical potential to the temporal evolution of ϕ:

$$\phi_t = \left(\phi^3 - \phi - \phi_{nn}\right)_{nn}. \quad (6)$$

The reader should notice that δ is not present in the previous equation and hereafter as a result of our aforementioned simplifications and strategy of non-dimensionalization. In this way, the chemical potential, θ, turns out $\theta = \phi^3 - \phi - \phi_{nn}$.

We are interested in the expressions of the resulting net stresses across the interface, $f^{(n)}$ and $f^{(s)}$, which result from the momentum equations due to the $\phi-$phase variations. This identification is realistic as we focus on a liquid jet flowing through a quiescent surrounding medium with a low-viscosity μ_o as $\mu \gg \mu_o$ and without any extra external force over the whole fluid system (i.e., finite interface and bulk). First, we write the coupled set of non-dimensional Cahn-Hilliard Navier-Stokes momentum equations, retaining each side's dominant contribu-

tion [18]

$$u_t^{(i)} + \epsilon\left(u^{(i)} - u^{(s)}\right)u_n^{(i)} + \epsilon\left(v^{(i)} - v^{(s)}\right)u_s^{(i)} + \quad (7a)$$
$$+ \frac{\rho p_n}{\rho_i} - \frac{\rho\mu_i u_{nn}}{\rho_i\mu} = -\frac{3\rho\kappa\phi_n^2}{2\sqrt{2}\rho_i}$$
$$v_t^{(i)} + \epsilon\left(u^{(i)} - u^{(s)}\right)v_n^{(i)} + \epsilon\left(v^{(i)} - v^{(s)}\right)v_s^{(i)} + \quad (7b)$$
$$\frac{\rho p_s}{\rho_i} - \frac{\rho\mu_i v_{nn}}{\epsilon^2\rho_i\mu} = \frac{3\rho\theta\phi_s}{2\sqrt{2}\rho_i},$$

where ρ_i, μ_i, $\kappa = 1/h + \mathcal{O}(\epsilon^2)$ are the inner density, viscosity of the interface and its first-order curvature, respectively, where μ_i is classically assumed to vary linearly with ϕ. Note that we take advantage of our previous scaling where ϵ and the squared-Cahn number are linked. The interface's slenderness also leads to having a dominant shear speed component (i.e. this statement could be better understood if we think in absolute coordinates) as we have $u^{(s)} = 0$ at both the liquid-interface boundary line and the outer streamline between the interface and environment. From the integration of Eqs. (7) along the normal direction as analogously was performed for a single outer length scale by Magaletti and coworkers [18], we obtain the first-order expressions of $f^{(n)}$ and $f^{(s)}$, being stresses that are ultimately transferred to the bulk through the boundary line in Eqs. (4):

$$f^{(n)} = \Delta(p_n) = \frac{3\kappa}{2\sqrt{2}}\int_0^\delta \phi_n^2 dn \quad (8a)$$
$$\epsilon f^{(s)} = -\Delta(v_{nn}) = \frac{3\epsilon^2\mu}{2\sqrt{2}}\int_0^\delta \frac{\theta\phi_s}{\mu_i}dn. \quad (8b)$$

We observe that the classical balances at the interface $f^{(n)} = \kappa$ and $f^{(s)} = 0$ are special cases of our more general approach towards an infinitely-narrow interface where $\phi^{ss} = \tanh(n/\sqrt{2})$ is the solution for the steady version of Eq. (6). In contrast, as we depart from the $\tanh-$solution, we have a $\phi-$dependent Laplace-Young expression and a non-zero, but much weaker than the latter, $O\left(\epsilon^2\right)$ shear stress in Eq. (8). Now we substitute the set of radially expanded variables of the bulk, Eq. (2) into Eq. (4), leading to the bulk-interface boundary equations in terms of stresses along normal and shear coordinates, respectively:

$$p_{0z} + v_{0z} = f^{(n)} \quad (9a)$$
$$-3v_{0z}h_z - v_{0zz}h + 2v_2 h = f^{(s)}. \quad (9b)$$

We substitute the variable expansion from Eq. (2) into the equation of motion for the streamline of the bulk boundary $h_t + vh_z = u$ along with the expressions for p_z and v_2 from Eqs. (9) and $f^{(n)}$, $f^{(s)}$ from Eqs. (8). Subsequently, from the evaluation of Eq. (3), we find a slender model for the liquid jet at the scale of the interface:

$$h_t + v_0 h_z = -\frac{1}{2}v_{0z}h \quad (10a)$$
$$v_{0t} + v_0 v_{0z} = \frac{3\left(v_{0z}h^2\right)_z}{h^2} + \frac{3}{2\sqrt{2}}\frac{h_z}{h^2}\int\phi_n^2 dn + \quad (10b)$$
$$+ \frac{3\epsilon\mu}{2\sqrt{2}h}\int\frac{\theta\phi_s}{\mu_i}dn + v_{0zz},$$

which corresponds to two equations for the unknowns $h(z,t)$ and $v_0(z,t)$ and a parametric dependence on $\phi(n,s,t)$ because $\phi_t \neq 0$ in Eq. (6). Note how the second, third and fourth terms on the right-hand side of Eq. (10b) respectively correspond to a diffusive surface tension stress, a non-zero interface shear stress, and the retainment of v_{ozz} from the classical expansion where it is systematically neglected. Indeed, this extra term v_{ozz} appears as we relax the zero free-shear stress boundary conditions of the classical slender model [19] towards a subdominant role in our formulation. The reader should notice how the set of the derived governing equations, although corresponding to two well-defined and separated regions of the fluid domain, are inherently linked through a spatio-temporal coupling within the pinching of the whole fluid system as the temporal dependence of ϕ creates a transient dynamics that prevents the stability of the classical steady-state solution in the finite-thickness interface.

Towards the singularity - Next, we seek the physical behavior of Eqs. (10) close to the pinch-off. For this reason, we take $t^* = t_b - t$ and $z^* = z - z_b$ as the time t^* and length z^* scales before the breakup. As $t^*, z^* \longrightarrow 0$, the change of variables

$$\xi = t^{*-1/2}z^* \quad (11a)$$
$$\eta = t^{*-1/4}n \quad (11b)$$
$$\phi = t^{*\chi}\Phi(\eta) \quad (11c)$$
$$h = t^{*(2\chi+3/4)}H(\xi) \quad (11d)$$
$$v_o = t^{*-1/2}V(\xi) \quad (11e)$$

enable us to balance the interface penalizing term with the temporal variation of ϕ along with the dominance of the stresses with origin in the diffusive surface tension over the interface shear contribution. Subsequently, both the bulk and finite interface are spatio-temporally tied, and from Eq. (6) and Eqs. (10) we find similarity equations

$$-\chi\Phi + \frac{\eta\Phi_\eta}{4} = -\Phi_{\eta\eta\eta\eta} \quad (12a)$$
$$-\left(2\chi + \frac{3}{4}\right)H + \frac{\xi H'}{2} = -\frac{1}{2}HV' - VH' \quad (12b)$$
$$\frac{V}{2} + \frac{\xi V'}{2} = -VV' + 4V'' + \frac{6V'H'}{H} + \frac{3H'}{2\sqrt{2}H^2}\int\Phi_\eta^2 d\eta, \quad (12c)$$

where $' = d/d\xi$. The three ordinary differential equations (12) describe two sub-spaces: the interface with

Eq. (12a), where Φ depends on η and parametrically on χ; and the bulk with ξ as the independent variable in the Eqs. (12b, 12c) that govern H, V, which are affected by the value of χ through both the prefactor of H in Eq. (12b) and the resulting varying surface tension stress. From Eq. (12b), we observe

$$H' = H\frac{\left(2\chi+\frac{3}{4}\right)-\frac{V'}{2}}{V+\frac{\xi}{2}}, \tag{13}$$

and consequently the existence of a certain value ξ_0 that makes H singular unless we also impose analytical properties to require $V_1 = V'(\xi_0) = (4\chi + 3/2)$.

Results - We construct a solution around ξ_0 as a Taylor series expansion for $H = \sum_{i=0}^{\infty} H_i(\xi - \xi_0)^i$ and $V = \sum_{i=0}^{\infty} V_i(\xi-\xi_0)^i$. Substituting them into Eqs. (12b), (12c) and after algebraic manipulations, we obtain the terms of order ξ^1 and ξ^2 for H and V, respectively

$$H_1 = \frac{9\xi_0 H_0^2}{H_0(9-8\chi)+\frac{3}{2\sqrt{2}}N} \tag{14a}$$

$$V_2 = \frac{9\xi_0 H_0(3-4\chi)}{H_0(9-8\chi)+\frac{3}{2\sqrt{2}}N}, \tag{14b}$$

where $N = \int \Phi_\eta^2 d\eta$. Note that Eqs. (14) only depends on ξ_0, H_0 and N, which are to be determined later. In addition, we derive a set of boundary conditions where the solution has to match the outer spatio-temporal scale at $\eta, \xi \longrightarrow \pm\infty$, making the left-hand terms of Eqs. (12) vanish due to their slow temporal origin and leading to the asymptotic behavior $\Phi \propto \eta^{4\chi}$, $H \propto \xi^{\left(4\chi+\frac{3}{2}\right)}$ and $V \propto \xi^{-1}$.

On the one hand, the family of solutions of Eqs. (12) within the interface is numerically obtained (Fig. 2) by the shooting method for the derived boundary conditions, where the values $N = 2\sqrt{2}/3$ and $\chi = 9/8$ set the domain that recovers the unity prefactor of the surface tension stress term in the classical *IV's* momentum equation. It is also interesting to note that the length of the self-similar domain in η is not infinite in a strict sense and has a cut-off of value, 15.6, (i.e. which was determined by machine-learning based numerical strategies) to ensure both odd-symmetry and only one inflexion point as the initial conditions from the base state solution impose when this pinch-off regime is triggered. However, this is far away enough to consider it as an approximation to ensure convergence to apply the aforementioned asymptotic boundary condition, with inspiration in classical works [5]. Then, we compute the resulting N by varying the value of χ in Eq. (12a). We observe that the morphology of the solution varies abruptly (Fig. 2) as $\chi < \chi_{min} \approx 0.745$, where N diverges. Indeed, the latter cases entail that interfacial velocities would reach infinite values that could not match the basic physical assumptions of the thinning jet and, consequently, are disregarded. We only consider the $N-\chi$ curve for $\chi > \chi_{min}$.

Now, we seek a pair (χ, N) that could lead to solutions of Eqs. (12b, 12c) that exhibit symmetry with respect to

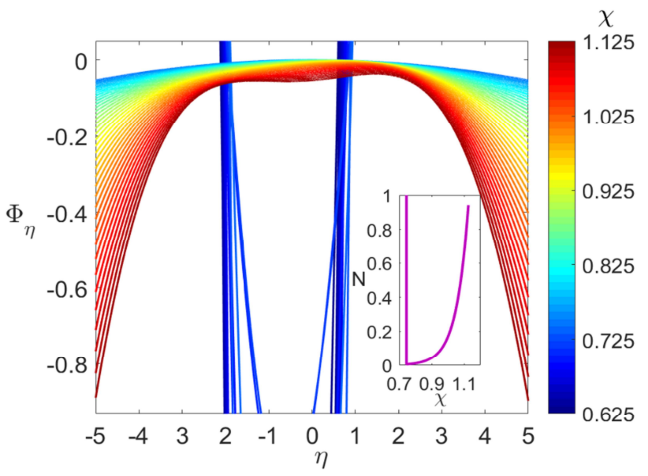

FIG. 2. Inner interfacial solutions of Φ_η for $\chi \in [0.625, 1.125]$. The inset shows the relation between N and χ, with a divergent behavior of N for $\chi < \chi_{min} = 0.745$ that corresponds to quasi-vertical blue curves in the main figure.

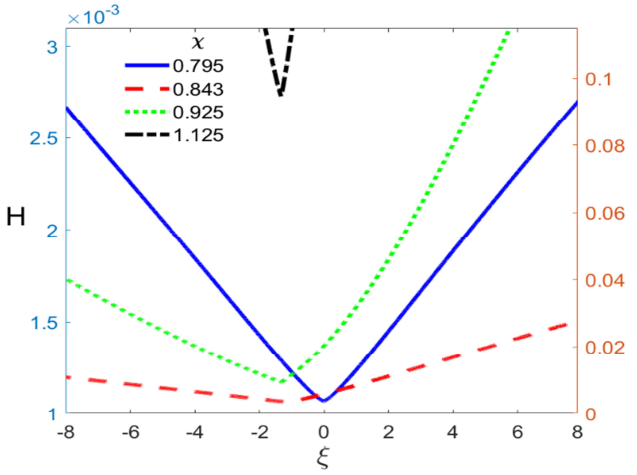

FIG. 3. Family of self-similar solutions for H as a function of χ. There is only an even symmetric profile (blue, solid line), for $\chi = 0.795$ (left vertical axis). The rest of the candidate curves are examples of how the symmetry is broken as χ varies (right vertical axis).

χ for the profiles of H and V, where we recall the same flow feature that on average takes place at the nanoscale [9] and also in larger-scaled pure diffusive experiments [12]. This strategy involves two parameters (χ, N) tied to the thermal interface roughening and the diffusive pinch-off, respectively, as the breakup radius and speed profiles turn out to be symmetric in the self-similar space of χ. We select the pair (χ, N) that is compatible with the latter features. To do so, we numerically solve Eqs. (12b, 12c) by the shooting method. For each (χ, N), firstly we assume the values (ξ_0, H_0) to evaluate the starting integration points for the branches of the solution on the right and left from ξ_0, by the expansion mentioned earlier

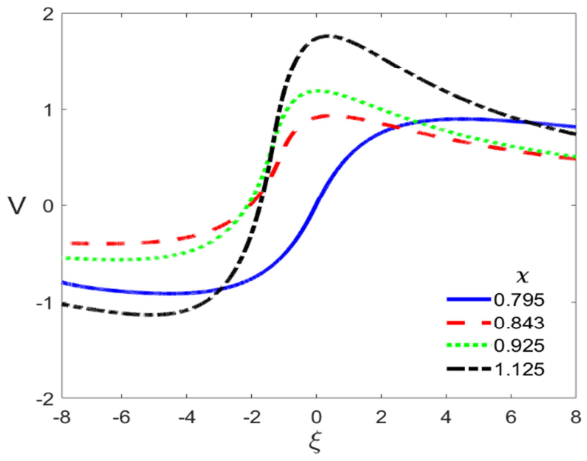

FIG. 4. Family of self-similar solutions for V as a function of χ. There is only an odd symmetric profile (blue, solid line), for $\chi = 0.795$. The rest of the candidate curves are examples of how the symmetry is broken as χ varies.

(Eqs. 14). Then we obtain a curve of candidate values of (ξ_0, H_0) for both branches that are compatible with the defined boundary conditions for $|\xi| \gg |\xi_0|$.

The global solution for a given pair (χ, N) is determined as both branches share the same location of the singularity ξ_0^* and its corresponding minimum thickness H_0^*. In these solutions, we check the intended symmetric profiles as a function of χ and its corresponding value of N. In particular, we observe in Fig. 3 how $H-$profiles become more symmetric as χ decreases. In addition, the smaller is the value of χ, the smaller is the minimum value of H, and the closer is ξ_0 to zero. Similar features occur with the respective $V-$profiles shown in Fig. 4, although in this case, the approach to symmetry is for an odd function instead of an even function. As χ decreases, $V-$profiles rotate clockwise as the singularity tends to move to zero. Ultimately, we find that the values $(\chi = 0.795, N = 0.00953, 2\chi + 3/4 \sim 2.34)$ lead to symmetric self-similar solutions for H and V, even and odd, respectively, along with $\xi_0 = -0.01$ and $H_0 = 0.00107$. Hence, we arrive at an expression of the evolution of the minimum neck radius $h_{min} = 0.00107(t_b - t)^{2.34}$. Thus, we have solved an open fundamental problem and provided keys for approaching a vast number of fluid phenomena that involve topological changes close to the continuum limit.

Prospects - Using the approach presented in this paper, it should be possible to address other open questions in jet-related fundamental problems:

1. The relation between the intact jet length and its instability [20], with a self-destabilizing loop close to the breakup region [21], to better appreciate the role played by transient pinch-off regimes.

2. The relation between pinch-off and recoil dynamics with the absence of satellite droplets in pure diffusive experiments [12, 13].

3. The role of interfacial fluctuations close to the continuum limit [9, 10] and whether or not they emerge before those that come from the bulk and, if so, how both energetic levels might compete within the fragmentation.

4. The extension of this work, together with the above points, to widely studied co-flowing streams [22–29] or electrosprays [30–34], where, probably below a specific scale, the finiteness of the Debye layer and diverse electrokinetic effects might appear [35].

F. C-M. acknowledges that this project has received funding from the European Union's Horizon 2020 research and innovation programme under the Marie Sklodowska-Curie grant agreement No 838997. We thank the NSF for support via CBET-1804863.

[1] J. Eggers and E. Villermaux, Physics of liquid jets, Rep. Prog. Phys. **71**, 036601 (2008).
[2] Z. Takáts, J. M. Wiseman, B. Gologan, and R. G. Cooks, Mass spectrometry sampling under ambient conditions with desorption electrospray ionization, Science **306**, 471–473 (2004).
[3] H. N. Chapman *et al.*, Femtosecond x-ray protein nanocrystallography, Nature **470**, 73–79 (2011).
[4] M. Gamero-Castaño and V. Hruby, Electrospray as a source of nanoparticles for efficient colloid thrusters, J. Propul. Power. **17**, 977–987 (2001).
[5] J. Eggers, Universal pinching of 3D axisymmetric free-surface flow, Phys. Rev. Lett. **71**, 3458–3460 (1993).
[6] J. R. Castrejón-Pita, A. A. Castrejón-Pita, S. S. Thete, K. Sambath, I. M. Hutchings, J. Hinch, J. R. Lister, and O. A. Basaran, Plethora of transitions during breakup of liquid filaments, Proc. Natl. Acad. Sci. **112**, 4582–4587 (2015).
[7] Y. Li and J. E. Sprittles, Capillary breakup of a liquid bridge: identifying regimes and transitions, J. Fluid Mech. **797**, 29–59 (2016).
[8] A. Deblais, M. A. Herrada, I. Hauner, K. P. Velikov, T. van Roon, H. Kellay, J. Eggers, and D. Bonn, Viscous effects on inertial drop formation, Phys. Rev. Lett. **121**, 254501 (2018).
[9] M. Moseler and U. Landman, Formation, stability, and breakup of nanojets, Science **289**, 1165–1169 (2000).
[10] J. Eggers, Dynamics of liquid nanojets, Phys. Rev. Lett. **89**, 084502 (2002).
[11] W. Kang and U. Landman, Universality crossover of the pinch-off shape profiles of collapsing liquid nanobridges in vacuum and gaseous environments, Phys. Rev. Lett.

98, 064504 (2007).
[12] Y. Hennequin, D. G. A. L. Aarts, J. H. van der Wiel, G. Wegdam, J. Eggers, H. N. W. Lekkerkerker, and D. Bonn, Drop formation by thermal fluctuations at an ultralow surface tension, Phys. Rev. Lett. **97**, 244502 (2006).
[13] J. Petit, D. Rivière, H. Kellay, and J. Delville, Break-up dynamics of fluctuating liquid threads, Proceedings of the National Academy of Sciences **109**, 18327–18331 (2012).
[14] H. Yung Lo, Y. Liu, S. Yi Mak, Z. Xu, Y. Chao, K. J. Li, H. Cheung-Shum, and L. Xu, Diffusion-dominated pinch-off of ultralow surface tension fluids, Phys. Rev. Lett. **123**, 134501 (2019).
[15] C. Zhao, D. Lockerby, and J. E. Sprittles, Dynamics of liquid nanothreads: Fluctuation-driven instability and rupture, Phys. Rev. Fluids **5**, 044201 (2020).
[16] J. W. Cahn and J.E. Hilliard, Free energy of a nonuniform system. i. interface free energy, J. Chem. Phys. **31**, 258–267 (1958).
[17] J. Lowengrub and L. Truskinovsky, Quasi-incompressible cahn–hilliard fluids and topological transitions, Proc. R. Soc. Lond. A **454**, 2617–2654 (1998).
[18] F. Magaletti, F. Picano, M. Chinappi, L. Marino, and C. M. Casciola, The sharp-interface limit of the cahn-hilliard/navier-stokes model for binary fluids, J. Fluid Mech. **714**, 95–126 (2013).
[19] J. Eggers and T. F. Dupont, Drop formation in a one-dimensional approximation of the Navier-Stokes equation, J. Fluid Mech. **262**, 205–221 (1994).
[20] S. Le Dizés and E. Villermaux, Capillary jet breakup by noise amplification, J. Fluid Mech **810**, 281–306 (2017).
[21] A. Unemura, Self-destabilising loop of a low-speed water jet emanating from an orifice in microgravity, Journal of Fluid Mechanics **797**, 146–180 (2016).
[22] J. R. Lister, Selective withdrawal from a viscous two-layer system, J. Fluid Mech. **198**, 231–254 (1989).
[23] A. M. Gañán-Calvo, Generation of steady liquid microthreads and micron-sized monodisperse sprays in gas streams, Phys. Rev. Lett. **80**, 285–288 (1998).
[24] I. Cohen, H. Li, J. L Hougland, M. Mrksich, and S. R. Nagel, Using selective withdrawal to coat microparticles, Science **292**, 265–267 (2001).
[25] S. L. Anna, N. Bontoux, and H. A. Stone, Formation of dispersions using flow focusing in microchannels, Appl. Phys. Lett. **82**, 364–366 (2003).
[26] A. S. Utada, E. Lorenceau, D. R. Link, P. D. Kaplan, H. A. Stone, and D. A. Weitz, Monodisperse emulsions generated from a microcapillary device, Science **308**, 537–541 (2005).
[27] A. S. Utada, A. Fernandez-Nieves, H. A. Stone, and D. A. Weitz, Dripping to jetting transitions in coflowing liquid streams, Phys. Rev. Lett. **99**, 094502 (2007).
[28] F. Cruz-Mazo, J. M. Montanero, and A. M Gañán-Calvo, Monosized dripping mode of axisymmetric flow focusing, Phys. Rev. E **94**, 053122 (2016).
[29] A. Dewandre, J. Rivero-Rodriguez, Y. Vitry, B. Sobac, and B. Scheid, Microfludic droplet generation based on non-embedded co-flow-focusing using 3d printed nozzle, Sci. Rep. **10**, 21616 (2020).
[30] G. Taylor, Disintegration of water drops in electric field, Proc. R. Soc. Lond. A **280**, 383–397 (1964).
[31] I. G. Loscertales, A. Barrero, I. Guerrero, R. Cortijo, M. Marquez, and A. M. Gañán-Calvo, Micro/nano encapsulation via electrified coaxial liquid jets, Science **295**, 1695–1698 (2002).
[32] A. M. Gañán-Calvo, J. M. López-Herrera, and P. Riesco-Chueca, The combination of electrospray and flow focusing, J. Fluid Mech. **566**, 421–445 (2006).
[33] R. T. Collins, K. Sambath, M. T. Harris, and O. A. Basaran, Universal scaling laws for the disintegration of electrified drops, PNAS **110**, 4905–4910 (2013).
[34] F. Cruz-Mazo, M. O. Wiedorn, M. A. Herrada, S. Bajt, H. N. Chapman, and A. M. Gañán-Calvo, Aerodynamically stabilized taylor cone jets, Phys. Rev. E **100**, 031101 (2019).
[35] A. Gupta, P. J. Zuk, and H. A. Stone, Charging dynamics of overlapping double layers in a cylindrical nanopore, Phys. Rev. Lett. **125**, 076001 (2020).